DeMPAA: Deployable Multi-Mini-Patch Adversarial Attack for Remote Sensing Image Classification

Jun-Jie Huang[†], *Member, IEEE*, Ziyue Wang[†], Tianrui Liu*, Wenhan Luo, *Senior Member, IEEE*, Zihan Chen, Wentao Zhao*, and Meng Wang, *Fellow, IEEE*

***Abstract*—Deep Neural Networks (DNNs) have demonstrated excellent performance in image classification, yet remain vulnerable to adversarial attacks. Generating deployable adversarial patches represents a promising approach to safeguard critical facilities against DNN-based classifiers used for Remote Sensing Images (RSI). While existing adversarial patch attack methods are designed for natural images, they typically generate a single and large patch which is impractically oversize for RSI applications. In this paper, we propose a Deployable Multi-Mini-Patch Adversarial Attack (DeMPAA) method for RSI classification task, which deploys multiple small adversarial patches on key locations considering both the feasibility and the effectiveness. The proposed DeMPAA method formulates the problem as a constrained optimization problem that jointly optimizes patch locations and adversarial patches. The proposed DeMPAA method takes a searching and optimization strategy to tackle it. The DeMPAA framework consists of a Feasible and Effective Map Generation (FEMG) module and a Patch Generation (PG) module. The FEMG module generates a location map to guide the adversarial patch location sampling by excluding the infeasible locations and considering the location effectiveness. In the PG module, a Probability guided Random Sampling based patch location selection (PRSamp) method is used to search better locations, then we optimize the adversarial patches using gradient descent with respect to an adversarial classification loss and an imperceptibility loss. Extensive experimental results conducted on Aerial Image Dataset show that the proposed DeMPAA method achieves 94.80% attacking success rate against ResNet50 using 16 small patches, which significantly outperforms other adversarial patch methods.**

***Index Terms*—Remote sensing image, classification, Adversarial patch attack**

I. Introduction

Deep Neural Networks (DNNs) have achieved superior performance on Remote Sensing Image (RSI) classification [1]–[3], and hence enable automatic classification on large scale RSI. Meanwhile, DNN-based classification also poses a great security concern when the targets in remote sensing scenarios are critical facilities that need to be protected from recognition. Considering that DNNs are vulnerable to adversarial attacks, adversarial attack methods can be of great value in protecting such critical facilities from DNN-based RSI classification. The adversarial attack methods generate adversarial examples by adding adversarial perturbation which is optimized with respect to the adversarial loss to the benign image [4]–[6]. The generated adversarial examples can then fool the DNN classifier, leading to an erroneous predicted class label.

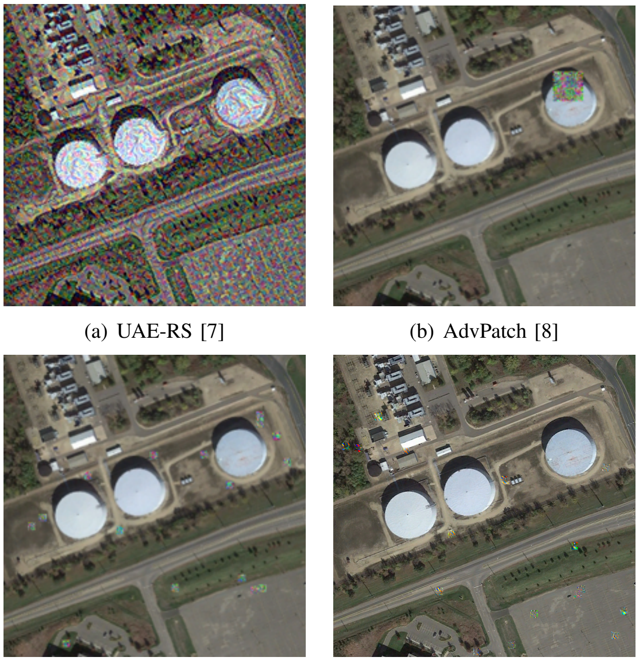
(a) UAE-RS [7]
(b) AdvPatch [8]
(c) DeMPAA (Ours)
(d) DeMPAA-IP (Ours)

Fig. 1. Visualization of adversarial examples generated by different adversarial attack methods. (a) UAE-RS [7] generates dense and noticeable adversarial perturbation on every pixel of the input image, (b) AdvPatch [8] pastes a single and large adversarial patch on the input image. The size of this patch is around 1% of the image size and the location of this patch is partially on the oil tank which is difficult to be deployed in practice. (c) The proposed DeMPAA realizes depolyable adversarial attack with 16 small adversarial patches selected according to a feasible and effective map. (d) Our DeMPAA-IP generates more imperceptible adversarial patches relying on additional imperceptible loss.

Adversarial attack methods have been investigated for RSI classification. Xu *et al.* [9] systematically analyze the threat of adversarial attack on DNN-based RSI classification and show that adding subtle adversarial perturbation to RSI can lead to misclassification with high confidence. Chen *et al.* [10] conduct a comprehensive investigation to the effect of adversarial examples on the RSI classification task and reveal the universality and severity of the adversarial example problem.

J.-J. Huang, Z. Wang, T. Liu, Z. Chen, and W. Zhao are with the College of Computer Science and Technology, National University of Defense Technology, Changsha, China. (E-mail: trliu@nudt.edu.cn).

W. Luo is with the Hong Kong University of Science and Technology, Hong Kong, China. (E-mail: whluo@ust.hk).

M. Wang is affiliated with the School of Computer Science and Information Engineering, Hefei University of Technology, Hefei, China. (E-mail: eric.mengwang@gmail.com).

[†]These authors contributed equally to this work.

*Corresponding author.

Xu *et al.* [7] propose a Mixup-Attack method for black-box adversarial attack to seek the common vulnerabilities of different DNNs which is termed as Universal Adversarial Examples in Remote Sensing (UAE-RS). The above RSI adversarial attack methods [7], [9], [10] mainly investigate digital adversarial attack approaches to deceive the DNN-based RSI classification models. These methods impose adversarial perturbations on every pixel of a remote sensing image, which is impractical in the real world to deploy the dense and additive adversarial noise everywhere.

In order to obtain deployable adversarial attack for remote sensing scenes, the number of modifications made to the original RSI should be limited to an acceptable amount. The sparse adversarial attack methods [11]–[15] have been proposed to restrict the adversarial perturbation to be sparse, aiming to improve the imperceptibility of the adversarial examples. The sparse adversarial attack approaches seem to be a promising option for depolyable adversarial attack for RSI. However, perturbing even 0.1% of pixels on a remote sensing image still requires to change the pixel values on hundreds of locations. Therefore, it is still challenging to physically implement the sparse adversarial attack methods on RSI applications.

The adversarial patch (AdvPatch) attack approach [8] generates adversarial examples by applying an optimized adversarial patch on the image to fool the DNN-based image classifier. In comparison to other aforementioned adversarial attack methods, the AdvPatch attack only requires deploying a single adversarial patch instead of perturbing pixel values on hundreds of independent locations. This characteristic increases its practicality for real-world implementation. Since the propose of AdvPatch by Brown *et al.* [8], it has been practically applied in many real scenarios, including face recognition [16]–[18], autonomous driving [19], [20], pedestrian detection [21]–[23], remote sensing image object detection [24], [25], etc.

Despite the success of adversarial attack methods, it is still challenging to achieve depolyable adversarial attack on the RSI classification task. The deployability of the model should balance between the size of feasible region and the number of patches. The size of feasible reign for deployment directly relates to the attacking capability, while the number of patches relates to the difficulty for deployment. Fig. 1 shows a visual comparison of different adversarial attack methods on an exemplar RSI. In Fig. 1(a), the UAE-RS method [7] generates universal adversarial examples with dense noise on every image pixel, which is impractical to be deployed in a real scene. In Fig. 1(b), the AdvPatch method [8] generates adversarial patches that are of 1% size of the image. Such patch size for RSI corresponds to a physical size of over 30×30 square meters, which is too large to be easily deployed in the real scene. Besides, the generated patch is partially located on the oil tank, which is difficult to deploy in practice. There are also adversarial attack methods which generate adversarial examples by perturbing a few number of pixels such as l_0-RS [13]. For l_0-RS [13] method, 1000 pixels need to be perturbed. Although those 1000 perturbed pixels are imperceptible on the RSI, such a large number of perturbation points can hardly be deployed in practice.

From the above we can see that the existing adversarial attack methods still face significant challenges when applied to RSI applications. For one thing, the existing adversarial patch methods have primarily been developed for natural images and often require a relatively large patch to ensure a high success rate in attacking the classifier. However, the practical deployment of adversarial patches in RSI classification requires minimizing their physical size, placing a constraint on the size of the patch. This presents a dilemma in RSI applications where a small patch may not be conducive to achieving a high attacking success rate, whereas a large patch might be challenging to deploy in real-world settings. Furthermore, the application of the adversarial patch is limited to specific regions within a scene due to practical constraints. For instance, it is difficult to deploy the patch on areas such as trees, cars, or bodies of water. To the best of our knowledge, there is currently a lack of research focus on exploring physically realizable adversarial patch attack methods specifically for RSI classification.

In this paper, we propose a simple and effective Depolyable Multi-Mini-Patch Adversarial Attack (DeMPAA) method for Remote Sensing Image (RSI) classification to tackle the aforementioned problems. Our goal is to design a robust and practically deployable adversarial attack method for RSI classification. To achieve this, we propose a novel DeMPAA method which selects a small number of physically deployable key locations on RSI to deploy multiple small adversarial patches. This ensures that each individual adversarial patch is small enough to be physically deployed in practical locations, while maintaining a high attacking success rate. Specifically, a Feasible and Effective Map Generation (FEMG) module is used to determine a patch location map with the reference to a feasibility map guided by a Feasible Region Selection Network (FRSNet) and an effectiveness map guided by the backpropagated loss. The Patch Generation (PG) module uses a Probability guided Random Sampling (PRSamp) method to sample n key patch locations for deploying the adversarial patches and then optimizes the n adversarial patches with respect to an adversarial classification loss and an imperceptibility loss. Relying on the cooperation of the FEMG module and the PG module, the proposed DeMPAA method can work with a searching and optimizing strategy to select both practically deployable and effective patch locations for robust and imperceptible adversarial attacks.

The contribution of this work is mainly three-fold:

- We propose a novel Deployable Multi-Mini-Patch Adversarial Attack (DeMPAA) method for RSI classification. Instead of using a single large adversarial patch, we propose to search and optimize multiple small adversarial patches for robust and deployable adversarial attack.
- In the proposed DeMPAA method, a Feasible and Effective Map Generation (FEMG) module determines a patch location map considering both the feasibility and the effectiveness, and a Patch Generation (PG) module then samples n key patch locations and optimizes the adversarial patches with respect to adversarial classification loss and imperceptible loss.
- From extensive experimental results, the proposed DeMPAA method achieves a significantly higher attacking success rate when compared to other methods, and

an imperceptible version of the proposed method *i.e.,* DeMPAA-IP generates even more visually imperceptible adversarial patches to be practically feasible for attacking RSI scenes.

The rest of the paper is organized as follows: Section II briefly reviews the related work in adversarial attack methods. Section III first formulates the optimization problem, and then introduces the proposed DeMPAA method in details. Section IV shows comparison results on two commonly used remote sensing datasets and presents ablation studies and discussions to further investigate the properties of the proposed method. Finally, Section V draws conclusions.

II. Related work

A. Digital Adversarial Attack

Most existing adversarial attacks generate adversarial examples in the digital domain to mislead the DNN classifier [4]–[6], [26]–[28]. Given a benign image $\boldsymbol{x}$ and the corresponding ground-truth label y, they aim to mislead the classifier $f_{\boldsymbol{\theta}}(\cdot)$ by adding adversarial perturbation on $\boldsymbol{x}$. The adversarial attack methods can be divided into targeted and untargeted attack methods. The targeted adversarial attack method generates adversarial example $\boldsymbol{x}_{adv}$ with an identified target class label, and the untargeted adversarial attack methods aim to mislead to the classifier to any other wrong class label. The Fast Gradient Sign Method (FGSM) [4] generates adversarial examples by adding adversarial perturbation in the direction of the sign of gradient, while the Projected Gradient Descent (PGD) method [26] takes an iterative manner with a smaller step size to achieve a more refined generation of adversarial examples. Deepfool method [5] aims to find the classification boundary hyperplane and move $\boldsymbol{x}$ to the hyperplane to fool the classifier with minimum perturbations. C&W method [27] formulates the adversarial attack as a constrained optimization problem to find minimum perturbations. Luo *et al.* [28] introduce a constraint on low-frequency sub-bands between benign and adversarial images, which encourages to generate more imperceptible adversarial examples. Chen *et al.* [6] propose to generate adversarial examples via Invertible Neural Networks by both adding and dropping semantic information which makes the distortions more imperceptible for human perception. Though taking different strategies, the digital adversarial attack methods require perturbing almost all pixel value on the image, and therefore can face difficulty in transferring the adversarial perturbations to the physical domain.

B. Sparse Adversarial Attack

To improve the imperceptibility of adversarial attacks, sparse attack methods are introduced to change as few pixels as possible by restricting the perturbation with a l_0-norm [11]–[15]. Modas *et al.* [11] propose a geometry inspired sparse attack method and approximate the decision boundary as an affine hyperplane to compute the sparse perturbations. Croce *et al.* [12] propose to craft adversarial examples by minimizing l_0-norm between the adversarial image and the original image and adding perturbations in region of high variation. Hein *et al.* [13] propose a Random Search (RS) strategy to optimize the sparse perturbation, termed as l_0-RS. By designing specific sampling distributions, l_0-RS method only needs to change 0.1% to 0.3% pixels to fool the classifiers. He *et al.* [15] propose to generate transferable sparse adversarial attack by generating the locations and values of the adversarial perturbation with two decoder networks. Zhu *et al.* [14] propose a homotopy algorithm to generate sparse perturbations as well as restrict the perturbation bound in one unified framework. Although sparse adversarial attack methods significantly reduce the number of perturbations, it is still challenging to deploy hundreds of perturbations in the physical world.

C. Adversarial Patch Attack

The adversarial patch attack approach is widely applied for physical attacks. An adversarial example can be obtained by pasting an adversarial patch on the image or on the object. Therefore, it is more feasible to implement in real scene. In the seminal work, Brown *et al.* [8] propose the Adversarial Patch (AdvPatch) method to learn a universal patch which can be pasted on all images to fool the deep classifiers. AdvPatch utilizes an adversarial patch of 5% image size which is acceptable for natural images but is too large to attack RSI in real scene. Wei *et al.* [18] propose to simultaneously optimize the adversarial patch and its position based on reinforcement learning for attacking the face recognition network. Kevin *et al.* [19] utilize the adversarial patch to attack the autonomous driving system by searching a suitable position to paste special stickers on traffic signs. Hu *et al.* [23] aim to attack pedestrian detectors by optimizing a naturalistic patch within the latent manifold of a pretrained Generative Adversarial Network. Fu *et al.* [29] prove the effectiveness of adversarial patch attack on vision transformers and select the location with the guidance of corresponding saliency map termed as Patch Fool (PFool). Li *et al.* [30] propose an end-to-end differentiable adversarial patch attack method termed as Generative Dynamic Patch Attack (GDPA) which employs a generator to produce the patch pattern and decides the location with reduced inference time. The existing adversarial patch methods mainly investigate to optimize a single adversarial patch and decide its position to generate adversarial images, since it is in general acceptable to paste a large patch on the natural image.

D. Adversarial Attack on RSI

There are adversarial attack methods designed for the RSI applications. For RSI image classification task, Burnel *et al.* [31] generate untargeted natural adversarial examples based on Wasserstein Generative Adversarial Networks [32] and achieve high transferability over different DNN classification models. Xu *et al.* [7] use a surrogate model to extract the shallow feature of clean images and mix-up images, and generate universal adversarial examples for RSI classification by adding perturbations to the benign images. These works are extensions of the digital adversarial attack methods on RSI classification task, however, these methods are difficult to be impracticable in the physical world. There are recent works that propose to apply adversarial patch attack on the RSI object detection task. Zhang *et al.* [24] find that the size of objects in RSI varies, therefore they propose to generate a universal adversarial patch that can adapt to multi-scale objects. They formulate a joint optimization problem to attack as many objects as possible and use a scale factor to adapt to objects with various sizes. Lian *et al.* [25] propose Adaptive-Patch-based Physical Attack (AP-PA) method for aerial detection to place the adversarial patch both on the object and outside the object. To the best of our knowledge, there are few works that investigated depolyable adversarial attack for RSI classification. The major challenging is how to achieve high adversarial attacking success rate while making the adversarial attack feasible for deployment.

III. Proposed Method

In this paper, we propose a novel DeMPAA for RSI classification with the objective to generate robust and depolyable adversarial examples. The core idea is, instead of generating a single large adversarial patch which is difficult to deploy due to its large physical size, we propose to generate multiple small adversarial patches on key locations.

A. Problem Formulation

Given a benign remote sensing image $\boldsymbol{x}$, the objective of this work is to paste multiple adversarial patches on $\boldsymbol{x}$ to mislead the deep image classification network of RSI. We leverage a mask image $\mathbf{M}$ and a patch image $\mathbf{P}$ which are of the same size of the benign image $\boldsymbol{x}$ to represent our adversarial image. The region to paste the adversarial patches is denoted by a binary mask image $\mathbf{M}$ where the patch region is with value 1 and otherwise. The adversarial patches $\{\mathbf{p}_i\}$ are of size $s \times s$. The adversarial image $\boldsymbol{x}_{adv}(\mathbf{M}, \mathbf{P})$ can thus be expressed as:

$$\boldsymbol{x}_{adv}(\mathbf{M}, \mathbf{P}) = (\mathbf{1} - \mathbf{M}) \odot \boldsymbol{x} + \mathbf{M} \odot \mathbf{P}, \tag{1}$$

where $\mathbf{1}$ is an all-ones matrix, and $\odot$ denotes the Hadamard product, $\mathbf{M}$ and $\mathbf{P}$ are both with the same size of the image $\boldsymbol{x}$.

In this paper, we mainly focus on untargeted adversarial attack, *i.e.,* to minimize the probability that the generated adversarial image is classified to the correct class label, that is, to misguide deep image classification networks to predict any of the wrong class labels. The optimization objective for DeMPAA can then be expressed as:

$$\arg \min_{\{\mathbf{M} \in \mathcal{F}, \mathbf{P} \in [0,255]\}} \mathcal{L}\left(f\left(\boldsymbol{x}_{adv}(\mathbf{M}, \mathbf{P}), y\right)\right), \tag{2}$$

where y is the ground-truth class label, $f(\cdot)$ denotes the target deep classifier, $\mathcal{F}$ represents a feasibility set of patch locations, and $\mathcal{L}$ denotes the loss function. For adversarial patches to be effective in the physical world, it is crucial that the value of $\mathbf{P}$ should be fall within the range of [0,255].

From Eqn. (2), we can see that the objective function involves the optimization of both the patch locations $\mathbf{M}$ and the adversarial patches $\mathbf{P}$, where the adversarial patches $\mathbf{P}$ depend on the patch locations $\mathbf{M}$. Such a bi-level optimization problem is generally difficult to optimize. In this paper, we propose to solve this problem with a searching and optimization strategy. That is, we first use a Feasible and Effective Map Generation (FEMG) Module to generate a feasible and effective location map which is used to guide the selection of the adversarial patch locations, then use a Patch Generation (PG) Module to search the locations of the adversarial patches $\mathbf{M}$ and to optimize the adversarial patches $\mathbf{P}$. The two modules will be introduced in details in Section III-C and Section III-D, respectively.

B. Overview of DeMPAA

Fig. 2 gives an overview of the proposed DeMPAA for RSI classification. It consists of a Feasible and Effective Map Generation (FEMG) module and a Patch Generation (PG) module. In the FEMG module, an effectiveness map $\mathcal{E}$ and a feasibility map $\mathcal{F}$ are generated to provide the location map $\mathcal{M}$ which is used to determine the adversarial patch locations considering both the feasibility and the effectiveness. Specifically, the effectiveness map $\mathcal{E}$ is obtained by feeding the benign image $\boldsymbol{x}$ into the target classifier using a guided back-propagation, the feasibility map $\mathcal{F}$ is obtained via a Feasible Region Selection Network (FRSNet). The black area on the feasibility map $\mathcal{F}$ represents the area unsuitable to deploy the adversarial patches. Then, the feasible and effective location map $\mathcal{M}$ is calculated by element-wise multiplication of $\mathcal{E}$ and $\mathcal{F}$. In the PG module, we calculate the selecting probability P with respect to $\mathcal{M}$ and sample n locations to settle the mask and use a gradient descent with backpropagation to update the adversarial patches with the given patch locations. In case that an attack fails, we use a resampling strategy to obtain a new set of patch locations with respect to $\mathcal{M}$.

C. Feasible and Effective Map Generation Module

We propose the Feasible and Effective Map Generation (FEMG) module to guide the optimization of the mask $\mathbf{M}$ in Eqn. (1). The optimization takes both the feasibility of the adversarial patch locations and the effectiveness of adversarial attack into consideration, relying on a physical feasibility map $\mathcal{F}$ and an attack effectiveness map $\mathcal{E}$, respectively.

Feasibility Map: The feasibility map $\mathcal{F}$ is generated by a Feasible Region Selection Network (FRSNet) which follows the pipeline of Object-Contextual Representation (OCR) [33]. It helps to exclude the locations that are unsuitable to deploy the adversarial patches in the real world locations, such as on ships, cars, trees or bodies of water. The FRSNet is trained on Dense Labeling Remote Sensing Dataset (DLRSD) [34] with 17 classes[1]. Among them, six of the classes, *i.e.*, *bare soil*, *dock*, *field*, *grass*, *pavement* and *sand*, are selected as the feasible locations which can deploy adversarial patches. The pixel values with feasible class labels are assigned to 1, and 0 otherwise to generate the feasibility map $\mathcal{F}$. A dilation operation according to the patch size $s \times s$ is applied to the semantic map in order to avoid overlapping with the boundary. The feasibility map $\mathcal{F}$ can be expressed as:

$$\mathcal{F} = \mathbf{1}_{s \times s} \circledast \Pi_{\mathbb{B}}(g(\boldsymbol{x})), \tag{3}$$

[1] airplane, bare soil, buildings, cars, chaparral, court, dock, field, grass, mobile home, pavement, sand, sea, ship, tanks, trees and water.

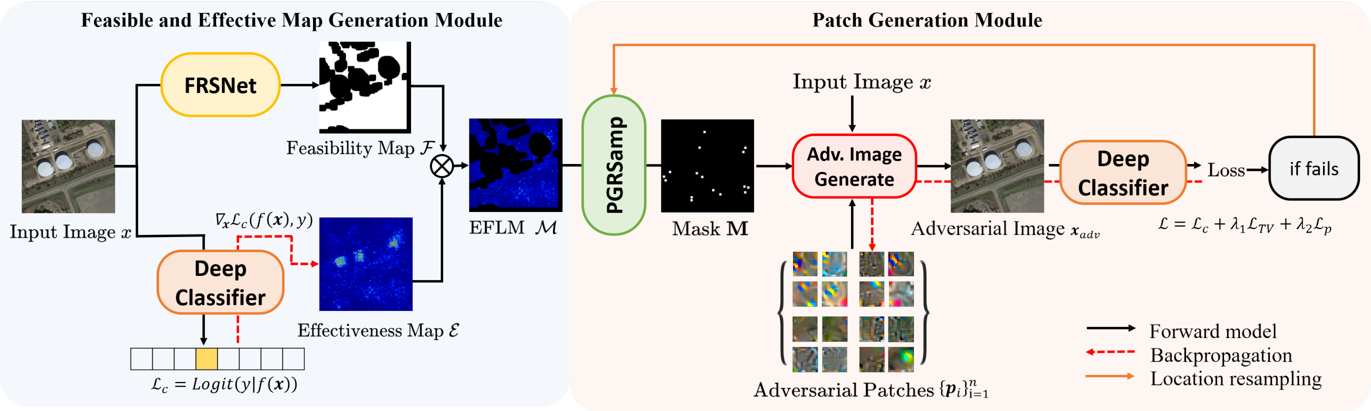
Feasible and Effective Map Generation Module
FRSNet
Feasibility Map $\mathcal{F}$
Input Image x
$\nabla_x \mathcal{L}_c(f(x), y)$
Deep Classifier
Effectiveness Map $\mathcal{E}$
$\mathcal{L}_c = Logit(y|f(x))$
EFLM $\mathcal{M}$
Patch Generation Module
PGRSamp
Mask $\mathbf{M}$
Input Image x
Adv. Image Generate
Adversarial Image x_{adv}
Deep Classifier
Loss
if fails
$\mathcal{L} = \mathcal{L}_c + \lambda_1 \mathcal{L}_{TV} + \lambda_2 \mathcal{L}_p$
Adversarial Patches $\{\boldsymbol{p}_i\}_{i=1}^n$
Forward model
Backpropagation
Location resampling

Fig. 2. Overview of the proposed Deployable Multi-Mini-Patch Adversarial Attack (DeMPAA) method for remote sensing image classification task. It consists of a Feasible and Effective Map Generation (FEMG) module and a Patch Generation (PG) module. In the FEMG module, an effectiveness map $\mathcal{E}$ and a feasibility map $\mathcal{F}$ are generated to provide the feasible and effective location map $\mathcal{M}$ to determine the adversarial patch locations considering both the feasibility and the effectiveness. In the PG module, according to $\mathcal{M}$, a Probability guided Random Sampling based patch location selection (PRSamp) method is proposed to generate a mask $\mathbf{M}$ with n sampled patch locations. A gradient descent with backpropagation is then used to update the adversarial patches $\{\mathbf{p}_i\}$ with the given mask. And if attack fails, a new set of patch locations will be resampled with respect to $\mathcal{M}$.

where $g(\cdot)$ denotes the OCR network, which outputs pixel-wise semantic labels, and $\Pi_{\mathbb{B}}(\cdot)$ is a binary projection operator which assigns the feasible locations to 1, and 0 otherwise, $\mathbf{1}_{s\times s}$ represents an all-one convolution kernel with size $s \times s$ and $\circledast$ represents the convolutional operator.

Effectiveness Map: We generate an effectiveness map $\mathcal{E}$ to indicate the contribution of the image region to the classification of the image. Specifically, we calculate the gradient of the loss function $\mathcal{L}_c$ for the input image $\boldsymbol{x}$. The magnitude of the gradient on each pixel indicates the potential effectiveness contributing to the generation of the adversarial image. The effectiveness map $\mathcal{E}$ can then be obtained by:

$$\mathcal{E} = \mathbf{1}_{s\times s} \circledast \left|\nabla_{\boldsymbol{x}} \mathcal{L}_c(f(\boldsymbol{x}), y)\right|, \tag{4}$$

where $\mathcal{L}_c$ denotes the adversarial classification loss function, which can be expressed as $\mathcal{L}_c(f(\boldsymbol{x}), y) = \text{Logit}\,(y \mid f\,(\boldsymbol{x}))$ denoting the logit output of $f(\boldsymbol{x})$ with respect to the target class y, and $\mathbf{1}_{s\times s}$ denotes an all-one convolution kernel which is used to calculate the sum of gradient values within the patch.

Feasible and Effective Location Map: To obtain a feasible and effective location map, denoted as $\mathcal{M}$, the impact of each pixel is evaluated and unsuitable locations are avoided. This is achieved through an element-wise product operation between the Feasibility Map $\mathcal{F}$ and the Effectiveness Map $\mathcal{E}$, *i.e.*, $\mathcal{M} = \mathcal{F} \otimes \mathcal{E}$. The black area in $\mathcal{M}$ is the region where patches cannot be placed, and the brighter the non-black area, the easier it will affect the classifier. We perform a probabilistic sampling with reference to the magnitude of $\mathcal{M}$, the specific method will be introduced in the next section.

D. Patch Generation Module

Given the feasible and effective location map $\mathcal{M}$, we use a Patch Generation (PG) Module to select the locations and optimize the multiple adversarial patches.

Patch Location Sampling: We propose a Probability guided Random Sampling based patch location selection (PRSamp) method to select the multiple small adversarial patch locations. In this work, we generate n small adversarial patches rather than a single large one. These n adversarial patches work in a mutual cooperative manner so that the optimization problem here is a combinatorial one and is difficult to be solved. A naive sampling strategy which directly selects the top-n gradient based on the $\mathcal{M}$ map cannot ensure the optimum solution. The proposed PRSamp method treats the values of $\mathcal{M}$ as guidance and selects patch locations based on probabilities. That is, the location with greater value has a higher probability to be selected. The PRSamp method uses softmax with temperature [35] to soft the contribution and calculate the probability as follows:

$$p_{i,j} = \frac{\exp\left(\mathcal{M}_{i,j}/t\right)}{\sum_{u,v} \exp\left(\mathcal{M}_{u,v}/t\right)}, \tag{5}$$

where (i, j) denotes the top left location of patch, $\mathcal{M}_{i,j}$ denotes the magnitude at (i, j), $p_{i,j}$ denotes the probability to select (i, j), and t represents the temperature hyper-parameter. We discuss the selection of t in detail in Section IV-D3.

Patch Optimization: Given the mask $\mathbf{M}$, the adversarial patches $\mathbf{P}$ are further optimized to fool the deep classifiers. $\mathbf{P}$ can be optimized *w.r.t.* Eqn. (2) with $\mathbf{M}$ being fixed. The values of patches $\mathbf{P}$ are initialized by adding Additive White Gaussian Noise (AWGN) $\boldsymbol{n} \sim \mathcal{N}(0, \sigma^2)$ with mean zero and variance σ^2 to the RSI patch values. Then gradient descent with backpropagation is used to update $\mathbf{P}$.

Resampling Strategy: Since a single random sampling attempt may not ensure successful attack, we propose a patch location resampling strategy. The patch locations will be resampled *w.r.t.* Eqn. (5) if the previously sampled locations do not lead to a successful attack. With this patch location resampling strategy, the proposed DeMPAA method can achieve improved attacking success rate with better patch locations. The adversarial attack will be considered as a successful attack and terminated if the output confidence of ground-truth label P_y is lower than a threshold $T = 10\%$. Otherwise a new set of patch locations will be resampled with respect to the location map $\mathcal{M}$.

E. Loss Functions

In this paper, we adopt two categories of loss terms to guide the patch generation. The first one is an adversarial classification (AdvC) loss, and the second one is an imperceptible loss which includes a Total Variation (TV) loss and a perceptual color (PerC) loss.

Adversarial Classification Loss: The adversarial classification loss is used to guide the generation of adversarial images with high attacking success rate. The logit output refers to the vector before applying the final softmax function when evaluating the CE loss. Following [36], the logit output with respect to the ground-truth label y is used to measure the output score of $f(\cdot)$. The AdvC loss can be expressed as:

$$\mathcal{L}_c = \text{Logit}\left(y \mid f\left(\boldsymbol{x}_{adv}(\mathbf{M}, \mathbf{P})\right)\right). \tag{6}$$

Imperceptible Loss: The visual imperceptibility of the adversarial patches is essential to protect the privacy of the critical facilities. The TV loss [37] and the PerC loss [38] are set to impose imperceptibility constraint on the generated adversarial patches.

The Total Variation (TV) loss encourages smoothness on the generated adversarial patches and reduces high-frequency components. It can be expressed as:

$$\mathcal{L}_{TV} = \sum_{i,j} \sqrt{(\boldsymbol{x}_{i,j-1} - \boldsymbol{x}_{i,j})^2 + (\boldsymbol{x}_{i+1,j} - \boldsymbol{x}_{i,j})^2}. \tag{7}$$

The PerC loss is set to improve the color imperceptibility of the adversarial patches. Instead of measuring distance in the original RGB color space, PerC measures the color distance in the CIELCH space which is better aligned with human visual perception. Specifically, the PerC loss can be expressed as:

$$\mathcal{L}_p = \left(\frac{\Delta L}{S_L}\right)^2 + \left(\frac{\Delta C}{S_C}\right)^2 + \left(\frac{\Delta H}{S_H}\right)^2 + \Delta R, \tag{8}$$

where $\Delta L, \Delta C, \Delta H$ are the distance between pixel values of the L (light) channel, C (chroma) channel and H (hue) channel in CIELCH space, $\Delta R = R_T \frac{\Delta C}{S_C} \frac{\Delta H}{S_H}$, and S_L, S_C, S_H, R_T are constant.

Therefore, the total loss function can be expressed as:

$$\mathcal{L} = \mathcal{L}_c + \lambda_1 \mathcal{L}_{TV} + \lambda_2 \mathcal{L}_p, \tag{9}$$

where λ_1 and λ_2 are regularization parameters to balance the imperceptibility and attacking success rate. In the following of the paper, let us denote the proposed DeMPAA method learned with the imperceptible loss as DeMPAA-IP.

The proposed DeMPAA method is summarized in Algorithm 1. Given a benign image $\boldsymbol{x}$ with the ground-truth label y, we first generate a feasible and effective map $\mathcal{M}$, then sample n patch locations guided probability p, and finally optimize the n adversarial patches with respect to the adversarial classification loss and the imperceptible loss using gradient descent with backpropagation.

IV. Experiments

In this section, we perform extensive experiments to verify the effectiveness of the proposed DeMPAA method. We first describe the experimental settings, then compare with state-of-the-art methods and present ablation studies and discussions.

Algorithm 1: DeMPAA

```
Input : benign image $\boldsymbol{x}$, classifier $f(\cdot)$, ground-truth
        label $y$, confidence threshold $T$, number of
        resampling attempts $K$, number of patches $n$,
        patch size $s \times s$, maximum iterations $N$;
Output: Adversarial image $\boldsymbol{x}_{adv}$;
Generate Effectiveness Map
  $\mathcal{E} \leftarrow \mathbf{1}_{s\times s} \circledast |\nabla_{\boldsymbol{x}} \mathcal{L}_c(f(\boldsymbol{x}), y)|$;
Generate Feasibility Map $\mathcal{F} \leftarrow \mathbf{1}_{s\times s} \circledast \Pi_{\mathbb{B}}(g(\boldsymbol{x}))$;
Generate Feasible and Effective Location Map
  $\mathcal{M} \leftarrow \mathcal{F} \otimes \mathcal{E}$;
Calculate probability $p_{i,j} \leftarrow \frac{\exp(\mathcal{M}_{i,j}/t)}{\sum_{u,v} \exp(\mathcal{M}_{u,v}/t)}$;
for $j = 0 \rightarrow K-1$ do
    Randomly initialize $n$ patches $\mathbf{P}$;
    Sample mask $\mathbf{M}$ w.r.t. probability $p$;
    for $l = 0 \rightarrow N-1$ do
        Update adversarial image
          $\boldsymbol{x}_{adv}(\mathbf{M}, \mathbf{P}) \leftarrow (\mathbf{1} - \mathbf{M}) \odot \boldsymbol{x} + \mathbf{M} \odot \mathbf{P}$;
        Update the loss function:
          $\mathcal{L}_c \leftarrow \text{Logit}\left(y \mid f\left(\boldsymbol{x}_{adv}(\mathbf{M}, \mathbf{P})\right)\right)$;
        Update the output confidence of $y$:
          $P_y \leftarrow \text{Softmax}(y \mid f(\boldsymbol{x}_{adv}(\mathbf{M}, \mathbf{P})))$;
        if $P_y > T$ then
            Update $\mathbf{P}$ by gradient descent with
              backpropagation;
        else
            Break;
        end
    end
    if $\boldsymbol{x}_{adv}$ is adversarial then
        Break;
    end
end
return: $\boldsymbol{x}_{adv}$.
```

A. Experimental Settings

1) Dataset: The Aerial Image Dataset (AID) [39] and the Remote Sensing Image classification dataset created by Northwestern Polytechnical University (NWPU-RESISC) [40] are used to evaluate the proposed method. AID has 10,000 images with 30 classes, and all images are of the resolution of 600×600. The NWPU-RESISC dataset has 31,500 images of 45 classes, and the image size is 256×256. The dataset has been randomly split into a training set and a testing set with a ratio of 7:3.

2) Classification Model: For AID, the pre-trained ResNet50[2] [41] is used as the target classifier, which achieves 3.83% top-1 error by further fine-tuning with the training dataset. We have also fine-tuned ResNet34, ResNet101 [41] and DenseNet121 [42] with 4.90%, 4.43% and 3.80% top-1 errors, respectively, to evaluate the performance of the proposed DeMPAA method. For NWPU-RESISC, we keep the default settings and the classifiers ResNet34, ResNet50,

[2] https://download.pytorch.org/models

TABLE I
THE ATTACKING SUCCESS RATE, PERCEPTUAL QUALITY AND AVERAGE PROCESSING TIME OF DIFFERENT ADVERSARIAL PATCH ATTACK METHODS AGAINST FOUR DIFFERENT CLASSIFIERS EVALUATED ON AID AND NWPU-RESISC. (THE BEST AND THE SECOND BEST RESULTS IN EACH COLUMN ARE IN BOLD AND UNDERLINED.)

Metrics	Methods	AID					NWPU-RESISC				
		ResNet34	ResNet50	ResNet101	DenseNet121	Average	ResNet34	ResNet50	ResNet101	DenseNet121	Average
ASR (%) ↑	AdvPatch [8]	69.12	71.48	66.32	61.15	67.02	71.25	50.51	73.43	69.24	66.11
	GDPA [30]	66.32	63.10	48.80	40.61	54.71	51.36	34.79	47.62	43.78	44.39
	PFool [29]	65.40	90.20	66.47	70.79	73.22	73.24	54.94	77.78	68.09	68.51
	DeMPAA-IP*	87.46	85.29	83.45	79.61	83.95	90.12	75.95	88.82	85.20	85.02
	DeMPAA*	**93.92**	**96.61**	**93.97**	**89.89**	**93.60**	**94.47**	**79.25**	**92.10**	**90.91**	**89.18**
LPIPS ↓	AdvPatch [8]	0.0597	0.0596	0.0596	0.0602	0.0598	0.1598	0.1673	0.1524	0.1669	0.1616
	GDPA [30]	0.0915	0.0915	0.0916	0.0976	0.0931	0.2419	0.2396	0.2454	0.2437	0.2427
	PFool [29]	0.0531	0.0525	0.0537	0.0594	0.0547	0.1398	0.1457	0.1469	0.1434	0.1440
	DeMPAA-IP*	**0.0425**	**0.0431**	**0.0440**	**0.0420**	**0.0429**	**0.1038**	**0.1048**	**0.1039**	**0.1091**	**0.1054**
	DeMPAA*	0.0537	0.0557	0.0558	0.0569	0.0555	0.1413	0.1558	0.1436	0.1498	0.1476
Time (s) ↓	AdvPatch [8]	12.5	12.1	12.7	13.2	12.6	12.8	13.9	13.1	14.8	13.7
	GDPA [30]	9.6	9.6	**10.1**	**10.3**	9.9	9.7	9.9	10.0	**10.1**	9.9
	PFool [29]	10.7	6.3	10.8	11.8	9.9	7.9	**8.1**	8.3	10.4	8.7
	DeMPAA-IP*	10.1	12.8	18.8	20.4	15.5	10.0	19.9	19.2	21.1	17.6
	DeMPAA*	**3.4**	**5.1**	**10.1**	11.7	**7.6**	**3.3**	9.1	**5.0**	11.9	**7.3**

* w/o FRSNet for fair comparison.

ResNet101 and DenseNet121 are fine-tuned with 6.17%, 5.31%, 5.48% and 4.77% top-1 errors, respectively.

3) Evaluation Metrics: We utilize the Attacking Success Rate (ASR) in percentage to evaluate the attacking performance. The Learned Perceptual Image Patch Similarity (LPIPS) [43] is used to evaluate the perceptual quality of the generated adversarial images. The average processing time is utilized to evaluate the efficiency of different methods. During testing, the images which cannot be correctly classified are discarded.

4) Settings for DeMPAA: We set the patch number as $n = 16$, the maximum number of resampling attempts $K = 3$ by default. For DeMPAA, we initialize the adversarial patches with random noise, and set the regularization parameters λ_1, λ_2 to zeros to achieve higher ASR and faster convergence speed. For the imperceptible version DeMPAA-IP, we initialized the adversarial patches by adding AWGN with standard deviation $\sigma^2 = 75$ to the original image patches, and set the regularization parameters to $\lambda_1 = 0.0025$ and $\lambda_2 = 0.005$ to generate more imperceptible adversarial examples. The optimizer used in the PG module is Adam [44] with the initial learning rate $2/255$ which is decayed every 200 iterations with decay rate 0.9. The maximum number of iterations is set to $N = 2000$, and the confidence threshold is set to $T = 10\%$ and used to ensure that the generated adversarial image is sufficiently misclassified. All experiments are performed on a computer with a NVIDIA RTX 3090 GPU of 24 GB memory, and the average memory consumption during code running is 8.0 GB. The code of the proposed method will be publicly available.

B. Comparisons to SOTA Methods

To evaluate the effectiveness of the proposed method, we compare the proposed DeMPAA method with the SOTA adversarial patch attack methods, including AdvPatch [8], GDPA [30] and PFool [29]. For fair comparison, the total patch size is set to 1% of image size.

Table I illustrates the ASR, LPIPS score and the average processing time of different adversarial attack methods against commonly used deep classifiers evaluated on AID and NWPU-RESISC. Since the comparison methods can paste the adversarial patch on any position, for fair comparison, here we show the results of the proposed DeMPAA method without using FRSNet to exclude the unsuitable locations. For the results of the complete DeMPAA, please refer to Table II.

From Table I, we can observe a similar trend of the results on two datasets. From the average results, the proposed DeMPAA method achieves the highest ASR as well as fast inference speed against all classifiers, and DeMPAA-IP achieves the best imperceptibility in terms of LPIPS. The AdvPatch [8] method optimizes a single adversarial patch with a randomly selected location which leads to around 25% lower ASR compared with DeMPAA against all classifiers evaluated on AID. This result validates the effectiveness of using multiple smaller adversarial patches. The GDPA [30] method uses a generator to generate the adversarial patch instead of gradient iteration approach and achieves a faster processing speed against ResNet101 and DenseNet121. However, GDPA achieves the lowest ASR among all methods. The PFool [29] method divides the benign image into a fixed number of blocks by the size of patches, then uses a saliency map to select the blocks and place the patches which restricts the flexibility of patch locations. Compared with PFool, the proposed DeMPAA method achieves 28.5%, 6.4%, 27.5% and 19.1% higher ASR on AID against ResNet34, ResNet50, ResNet101 and DenseNet121, respectively. This result also indicates that the proposed location selection method using effectiveness map information as a probabilistic guidance is effective. The DeMPAA-IP also achieves the second best ASR

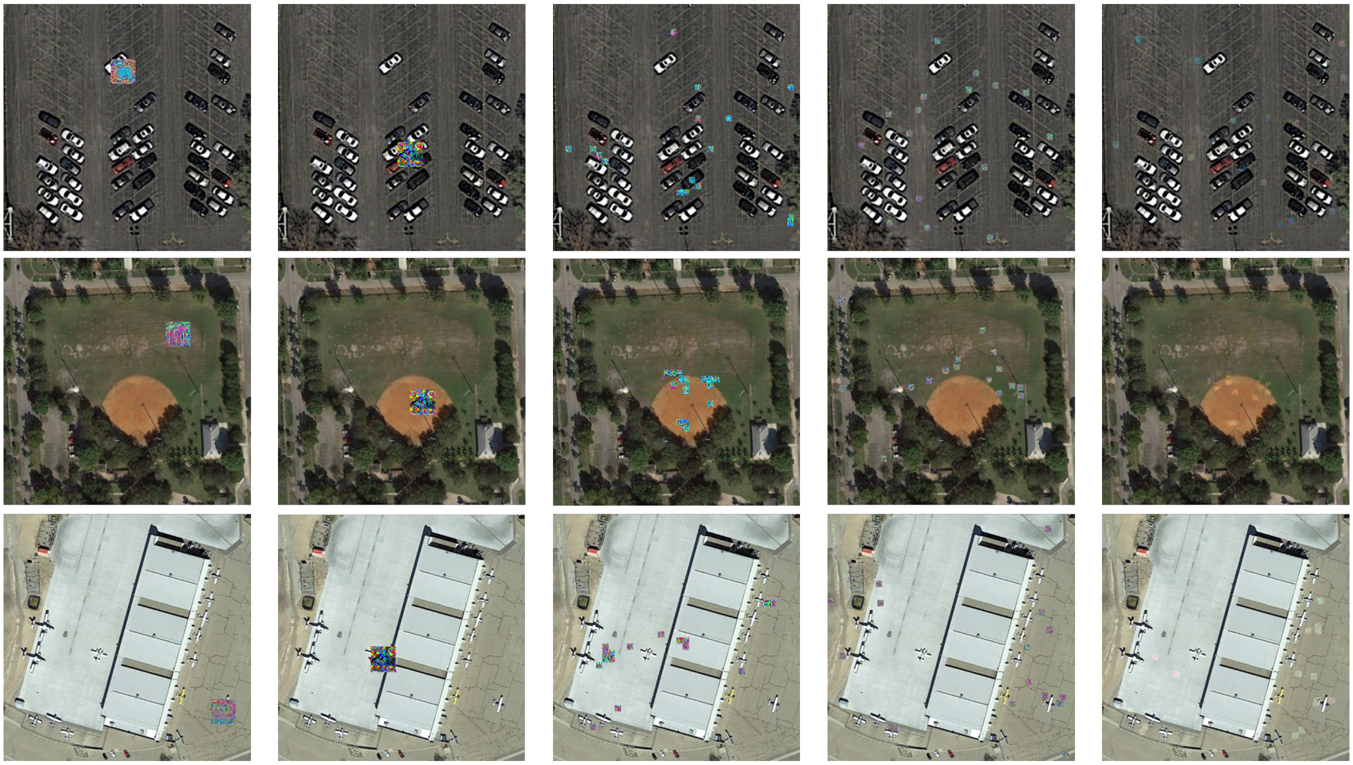

(a) AdvPatch [8] (b) GDPA [30] (c) PFool [29] (d) DeMPAA (Ours) (e) DeMPAA-IP (Ours)

Fig. 3. Three exemplar visualization result of different adversarial patch attack methods evaluated on the AID dataset. The total patch size is set to 1% of image size in all methods.

(except against ResNet50) and the best perceptual quality of the generated adversarial examples. Against all classifiers in AID, DeMPAA-IP achieves around 0.01 lower LPIPS score than PFool.

Fig. 3 shows the visualization results of different adversarial patch attack methods on AID against ResNet50. We can see that the adversarial examples generated by AdvPatch [8] and GDPA [30] are with a large and visible adversarial patch, the PFool [29] method are with a number of visible adversarial patches on grid, whereas the proposed DeMPAA method generates adversarial patches which are deployed on feasible locations, and DeMPAA-IP, *i.e.,* the proposed method with imperceptible loss further improves the imperceptibility for human perception.

C. Ablation Studies

To investigate the properties of DeMPAA method, we conduct ablation studies to investigate the effect of different components to the overall performance.

Network Structure: Table II shows the ablation study of the proposed DeMPAA method with respect to the proposed FRSNet for feasibility map generation, the proposed Probability guided Random Sampling based patch location selection (PRSamp) method, and the patch location resampling strategy. From Table II, we can see that the FRSNet would slightly reduce ASR (around 2%), but it can help the generated adversarial patches easier to be deployed in real scene. The proposed location selection method PRSamp can improve ASR and reduce processing time compared to randomly selecting the patch locations without any guidance. And the resampling strategy leads to an improved ASR which also slightly increases the processing time.

It is also interesting to note that, by increasing the number of patches, DeMPAA not only achieves a higher ASR, but also generates adversarial examples with a reduced processing time. This validates that the proposed DeMPAA leads to both improved effectiveness and efficiency. It can be noted that ASR consistently rises as the number of patches increases, but the improvements tend to diminish when the number of patches exceeds 16. If we keep increasing the number of patches, DeMPAA will be closer to a sparse attack, with a higher ASR, but harder to be deployed for the excessive patch numbers. Considering practical deployment difficulties and attacking success rates, we set patch number $n = 16$ by default.

Imperceptibility: In DeMPAA-IP, the TV loss imposes a smoothness constraint on the generated adversarial patches, and the PerC loss can further constrain the color of the adversarial patches to be more similar to the background. The visualizations of examples with and without imperceptible loss are shown in Fig. 4. We can see that with TV loss and PerC loss, the adversarial patches will be less perceptible and more similar to the background.

Fig. 5 shows the ablation study on weights of TV loss and PerC loss respect to the attacking success rate and LPIPS. We can see that both TV loss and PerC loss contribute to the imperceptibility of the generated adversarial patches.

TABLE II
ABLATION STUDY OF THE EFFECT OF DIFFERENT COMPONENTS IN DEMPAA METHOD. (W/O PRSAMP MEANS RANDOMLY SELECTING THE PATCH LOCATIONS WITHOUT ANY GUIDANCE.)

Settings			Metrics	Patch Number						
FRSNet	PRSamp	Resampling		1	2	4	8	16	24	32
✗	✓	✓	ASR(%)↑	79.05	87.08	92.23	93.42	96.61	97.15	97.22
			Time(s)↓	11.2	7.2	6.6	5.5	5.1	5.0	5.0
✓	✗	✓	ASR(%)↑	74.49	81.84	87.79	89.74	92.34	93.12	93.87
			Time(s)↓	11.9	10.2	7.6	6.6	6.6	6.5	6.4
✓	✓	✗	ASR(%)↑	69.72	77.62	84.49	89.01	91.37	92.01	92.48
			Time(s)↓	9.3	7.8	4.9	4.8	4.0	3.9	3.8
✓	✓	✓	ASR(%)↑	76.19	84.44	90.21	92.74	94.80	95.12	95.39
			Time(s)↓	10.5	9.4	6.5	6.4	6.1	6.1	6.0

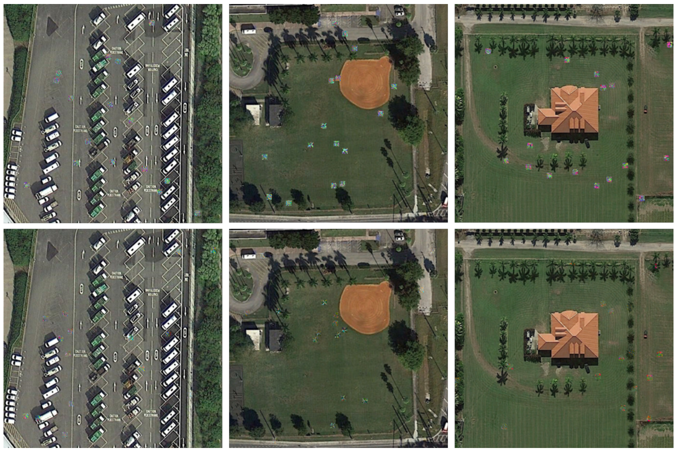

Fig. 4. Visualizations of the generated adversarial examples by DeMPAA (the 1-st row) and DeMPAA-IP with additional imperceptible loss (the 2-nd row).

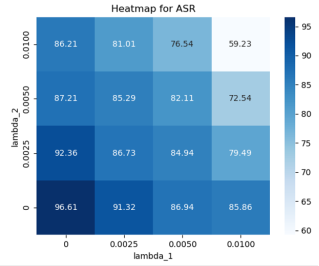

Fig. 5. The ablation study on weight choices for TV loss and PerC loss respect to attacking success rate (left) and LPIPS (right).

After comprehensively evaluating different combinations of λ_1 and λ_2, we set their default value to 0.0025 and 0.005, respectively, which achieves a good balance between ASR and imperceptibility.

Table III shows the impact of the strength of the added AWGN to the attacking performance and imperceptibility. We can observe that with an increase of noise level for initializing the adversarial patches, the generated adversarial examples will be less perceptible, but the attack will be more difficult to converge. In order to generate less perceptible adversarial examples as well as keep an acceptable ASR, we set $\sigma^2 = 75$ as the default setting for DeMPAA-IP.

TABLE III
THE ATTACKING SUCCESS RATE, PERCEPTUAL QUALITY AND AVERAGE PROCESSING TIME OF DEMPAA-IP WITH DIFFERENT NOISE LEVEL FOR INITIALIZATION.

σ^2	0	25	50	75	100
ASR(%)↑	69.29	73.34	79.25	83.24	88.34
LPIPS ↓	0.0325	0.0305	0.0386	0.0411	0.0479
Time(s)↓	30.7	27.1	26.7	15.1	11.2

TABLE IV
THE ADVERSARIAL ATTACK PERFORMANCE OF DIFFERENT LOCATION SELECTION METHODS WHEN USING DIFFERENT NUMBERS OF ADVERSARIAL PATCHES.

Method	Metrics	Patch number				
		1	2	4	8	16
APRSamp	ASR (%)↑	74.36	82.56	88.39	91.13	93.01
	Time (s)↓	11.9	10.1	9.7	8.3	7.4
PRSamp	ASR (%)↑	76.19	84.44	90.21	92.74	94.80
	Time (s)↓	10.5	9.4	6.5	6.4	6.1
APRSamp*	ASR (%)↑	79.42	84.19	90.05	94.18	96.98
	Time (s)↓	13.1	12.4	10.2	8.0	6.4
PRSamp*	ASR (%)↑	79.05	87.08	92.23	93.42	96.61
	Time (s)↓	11.2	7.2	6.6	5.5	5.1

* w/o FRSNet.

D. Discussions

1) Comparison with Previous Work: In our previous work [45], we propose a class activation map to guide random sampling based patch location selection (APRSamp) method to select the effective location of patches. It utilizes Grad-CAM [46] to locate the image region which has the greatest contribution to the classification. Table IV compares the effectiveness and efficiency of APRSamp method and PRSamp method. We can observe that PRSamp generates adversarial examples with a faster speed than APRSamp. When taking FRSNet into consideration, APRSamp achieves lower ASR than PRSamp. The reason is that APRSamp prefers to paste adversarial patches on the locations which attract much more attentions of the classifier. However, these areas are usually infeasible locations to deploy adversarial patches (*e.g.*, aircrafts in *airport*, cars in *parking*) which will be excluded by FRSNet. Fig. 7 shows the visualization of the gradient map and heat map of benign images with different scene categories,

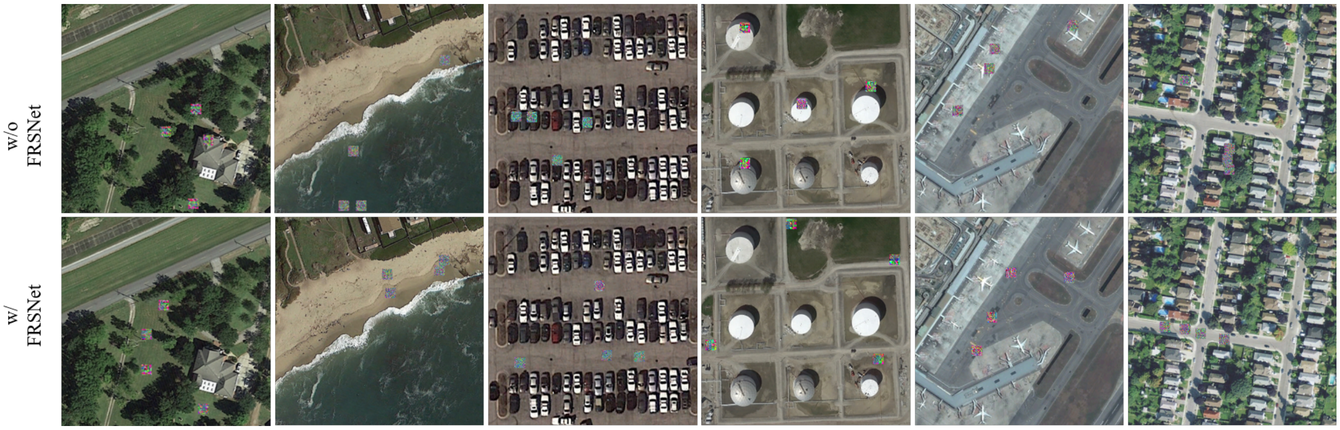

Fig. 6. Visualization of the generated adversarial examples by DeMPAA w/o FRSNet (the 1-st row) and w/ FRSNet (the 2-nd row). We use patch number $n = 4$ for illustration. Without using FRSNet, most adversarial patches are pasted on unsuitable areas.

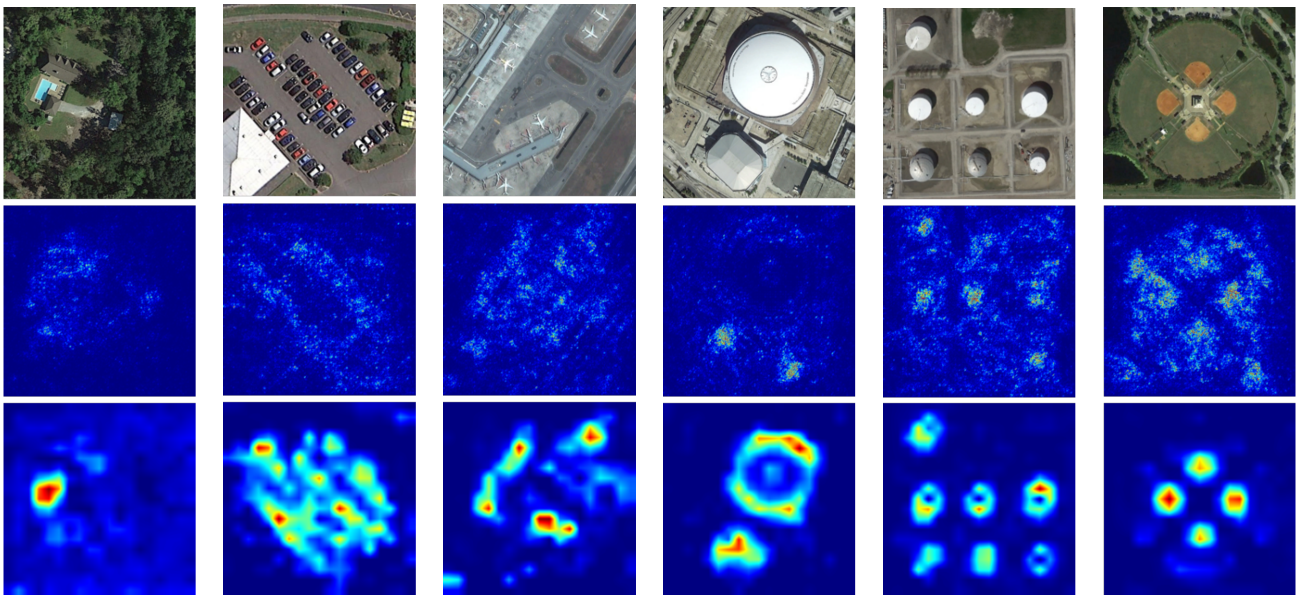

(a) *Sparse Residential* (b) *Parking* (c) *Airport* (d) *Center* (e) *Storage tanks* (f) *Baseball field*

Fig. 7. The gradient of the loss function for the input image (the 2-nd row) and the heat map generated by Grad-CAM (the 3-rd row) of benign images with different scene categories.

TABLE V
THE CROSS-MODEL TRANSFERABILITY OF DEMPAA. THE 1-ST COLUMN INDICATES THE TARGET CLASSIFIER FOR GENERATING ADVERSARIAL EXAMPLES. AND THE NUMBERS IN THE TABLE INDICATE THE FOOLING RATE (%) AGAINST OTHER CLASSIFIERS.

Models	ResNet34	ResNet50	ResNet101	DenseNet121
ResNet34	–	8.98	7.57	5.64
ResNet50	10.36	–	5.82	4.10
ResNet101	10.29	7.78	–	4.80
DenseNet121	15.71	10.66	9.13	–

TABLE VI
THE CROSS-MODEL TRANSFERABILITY OF DEMPAA WITH MODEL ENSEMBLE METHOD. THE 1-ST COLUMN INDICATES THE LEAVE-ONE-OUT ENSEMBLE MODEL AND '-' MODEL DENOTES THE SPECIFIC MODEL IS EXCLUDED FROM THE ENSEMBLE MODEL. THE NUMBERS IN THE TABLE INDICATE THE FOOLING RATE (%) AGAINST THE CORRESPONDING CLASSIFIER.

Models	ResNet34	ResNet50	ResNet101	DenseNet121
- ResNet34	54.05	88.89	86.01	75.91
- ResNet50	85.51	44.63	97.10	79.71
- ResNet101	92.48	87.61	40.71	67.70
- DenseNet121	90.61	85.39	89.77	19.87

we can observe that the values of heat map are denser than gradient map. Also, the areas that attract more attention may be excluded by FRSNet with a high probability.

2) The Transferablity of DeMPAA: We also evaluate the cross-model transferablity of the proposed DeMPAA method, and the results are shown in Table V. Specifically, we test the proposed DeMPAA on four models, including ResNet34, ResNet50, ResNet101 and DensNet121. We can observe that the adversarial examples generated by DeMPAA have low

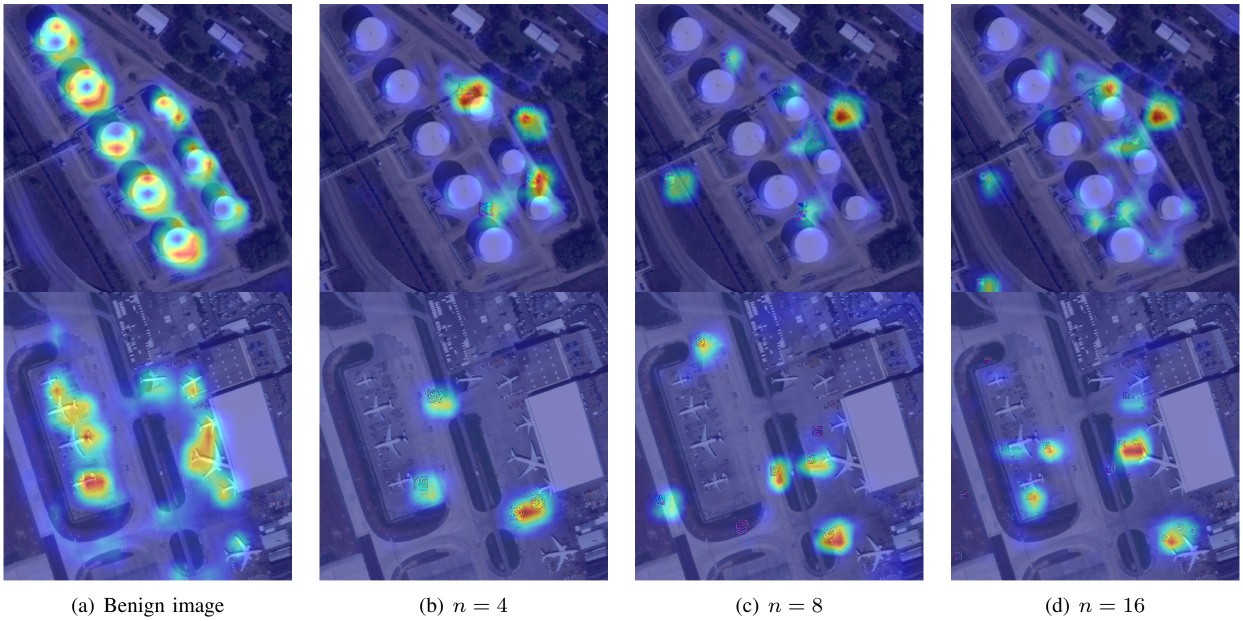

Fig. 8. Visualization of the heat maps of the adversarial examples generated by DeMPAA with different numbers of adversarial patches n. With the increasing number of patches, the attention transfers from the objects to the adversarial patches and becomes more scattered.

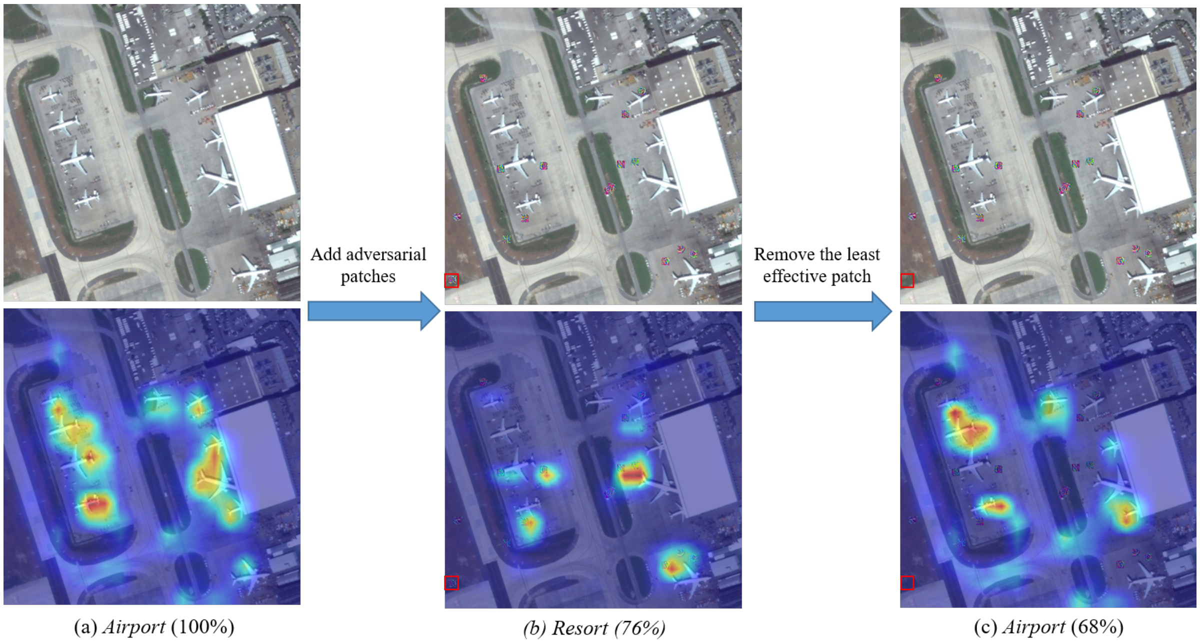

Fig. 9. Analysis on the effect of the adversarial patch with the least attention. The 1-st row represents the benign image, the adversarial image and the patch removed adversarial image, respectively. The 2-nd row denotes the corresponding heat map and the confidence of top-1 classification.

TABLE VII
THE ASR AND THE AVERAGE PROCESSING TIME OF DIFFERENT t IN EQN. (5) TO CALCULATE THE PROBABILITY IN PRSAMP METHOD.

Temperature	1	5	10	15	20
ASR (%)↑	90.28	92.48	94.80	94.12	94.04
Time (s)↓	7.4	6.4	6.1	6.2	6.2

transferablity cross models, especially when transferring to more complex model (only around 5% fooling rate transferring to DenseNet121 model). The possible reason is that our gradient-based optimization method makes the generated adversarial examples over-fit to the target model and common gradient-based attack methods face the same problem.

To improve the cross-model transferablity of the proposed method, the most common method is model ensemble. In details, the average gradients are utilized to guide the location selection and patch generation. And the termination condition is modified to that the output confidences of all methods are lower than the threshold $T = 10\%$. The results of DeMPAA with model ensemble are shown in Table VI. The values in the diagonal of the table indicate the transferablity from the ensemble model to the target black-box model. We can see that the adversarial examples achieve an acceptable transferablity (over 40%) on models with similar structures. But when the structure of target model is different from ensemble model (from ResNet to DenseNet), there is still much room for improvement.

3) Discuss about Temperature t: In the PRSamp method described in Section III-D, temperature t is an essential parameter to soft the distribution. Table VII shows the results of PRSamp method with different temperature settings. When $t = 1$, Eqn. (5) becomes a softmax function. By increasing the temperature parameter, we can observe an improved ASR and a reduced processing time. When t is larger than 10, the ASR begins to decline. Therefore, we choose $t = 10$ as our default setting.

4) Attention Transfer: The Grad-CAM [46] method can be used to visualize the heat map of the class activation of an input image. In this section, we utilize Grad-CAM to visualize the heat map transformation between the benign images and adversarial examples. The visualization results are shown in Fig. 8. The heat maps of two benign images with the ground-truth label *storage tanks* and *airport* are shown in the 1-st column in Fig. 8. We can see that the classifier mainly focuses on characteristics related to the class labels, *i.e.,* storage tanks and aircrafts. In Fig. 8(b), we show the heat map of adversarial images with $n = 4$ adversarial patches and can find that most of the attention has now been attracted to the deployed adversarial patches. In Fig. 8(c)-(d), the number of adversarial patches increases, and the heat map becomes more scattered. As we conjecture, this would be the reason why the proposed DeMPAA method has a higher attacking success rate when the number of adversarial patches increases.

In Fig. 8, we find that although most adversarial patches attract attention from the classifier, there are still certain adversarial patches attracting less attention. Therefore, we have further investigated whether these adversarial patches with less attention are necessary or not. We remove the least effective adversarial patch (marked in red box in (b)) as shown in Fig. 9. The result shows that after removing the least effective adversarial patch, the classification result changes from *Resort* with 76% confidence to *Airport* with 68% confidence and the heat map shows that the attention transfers back to the aircrafts. This indicates that different adversarial patches are collaborated to form an adversarial example and all contribute to the success of an adversarial attack.

V. Conclusions and Future Works

In this paper, we propose a novel Deployable Multi-Mini Patch Adversarial Attack (DeMPAA) method for RSI classification which utilizes multiple small and less perceptible adversarial patches to achieve physically feasible adversarial attack. The proposed DeMPAA consists of two main modules. The first module is Feasible and Effective Map Generation (FEMG) module, which employs a Feasible Region Selection Network (FRSNet) to generate a map with feasible and effective regions for sampling patch locations while excluding potentially unsuitable regions. The second module is the Patch Generation (PG) module, which utilizes a Probability guided Random Sampling based patch location selection (PRSamp) method to select patch locations and performs optimization of the adversarial patches using gradient descent. An imperceptible version DeMPAA-IP is also proposed to generate less perceptible adversarial examples using the TV and PerC loss. Extensive experimental results on the AID and NWPU-RESISC demonstrate that DeMPAA not only achieves a higher attacking success rate but also accelerates the attacking process.

For future works, a promising direction is to delve into multi-patch adversarial attack for black-box scenarios, which aligns closely with the practical applications. This would involve developing attack strategies that remain effective even when there is limited or no information about the target model. Furthermore, it is also essential to improve attacking robustness across a spectrum of environmental variables including fluctuations on lighting conditions, path locations, and diverse viewing perspectives.

Acknowledgment

This work is supported by the National Natural Science Foundation of China under Project 62201600, 62201604 and U1811462, NUDT Innovation Science Foundation 23-ZZCXKXKY-07, and NUDT Research Project ZK22-56.

References

[1] M. Rezaee, M. Mahdianpari, Y. Zhang, and B. Salehi, “Deep convolutional neural network for complex wetland classification using optical remote sensing imagery,” *IEEE Journal of Selected Topics in Applied Earth Observations and Remote Sensing*, vol. 11, no. 9, pp. 3030–3039, 2018.

[2] A. Ma, Y. Wan, Y. Zhong, J. Wang, and L. Zhang, “Scenenet: Remote sensing scene classification deep learning network using multi-objective neural evolution architecture search,” *ISPRS Journal of Photogrammetry and Remote Sensing*, vol. 172, pp. 171–188, 2021.

[3] X. Hu, Y. Zhong, X. Wang, C. Luo, J. Zhao, L. Lei, and L. Zhang, “Spnet: Spectral patching end-to-end classification network for uav-borne hyperspectral imagery with high spatial and spectral resolutions,” *IEEE Transactions on Geoscience and Remote Sensing*, vol. 60, pp. 1–17, 2022.

[4] I. J. G. S. Szegedy, “Explaining and harnessing adversarial examples,” *Statistics*, 2014.

[5] S.-M. Moosavi-Dezfooli, A. Fawzi, and P. Frossard, “Deepfool: a simple and accurate method to fool deep neural networks,” in *Proceedings of the IEEE Conference on Computer Vision and Pattern Recognition*, 2016, pp. 2574–2582.

[6] Z. Chen, Z. Wang, J. Huang, W. Zhao, X. Liu, and D. Guan, “Imperceptible adversarial attack via invertible neural networks,” in *Proceedings of the AAAI Conference on Artificial Intelligence*, vol. 37, no. 1, 2023, pp. 414–424.

[7] Y. Xu and P. Ghamisi, “Universal adversarial examples in remote sensing: Methodology and benchmark,” *IEEE Transactions on Geoscience and Remote Sensing*, vol. 60, pp. 1–15, 2022.

[8] T. B. Brown, D. Mané, A. Roy, M. Abadi, and J. Gilmer, “Adversarial patch,” *NIPS*, 2017.

[9] Y. Xu, B. Du, and L. Zhang, “Assessing the threat of adversarial examples on deep neural networks for remote sensing scene classification: Attacks and defenses,” *IEEE Transactions on Geoscience and Remote Sensing*, vol. 59, no. 2, pp. 1604–1617, 2020.

[10] L. Chen, Z. Xu, Q. Li, J. Peng, S. Wang, and H. Li, “An empirical study of adversarial examples on remote sensing image scene classification,” *IEEE Transactions on Geoscience and Remote Sensing*, vol. 59, no. 9, pp. 7419–7433, 2021.

[11] A. Modas, S.-M. Moosavi-Dezfooli, and P. Frossard, "Sparsefool: a few pixels make a big difference," in *Proceedings of the IEEE/CVF conference on computer vision and pattern recognition*, 2019, pp. 9087–9096.

[12] F. Croce and M. Hein, "Sparse and imperceivable adversarial attacks," in *Proceedings of the IEEE/CVF International Conference on Computer Vision*, 2019, pp. 4724–4732.

[13] F. Croce, M. Andriushchenko, N. D. Singh, N. Flammarion, and M. Hein, "Sparse-rs: a versatile framework for query-efficient sparse black-box adversarial attacks," in *Proceedings of the AAAI Conference on Artificial Intelligence*, vol. 36, no. 6, 2022, pp. 6437–6445.

[14] M. Zhu, T. Chen, and Z. Wang, "Sparse and imperceptible adversarial attack via a homotopy algorithm," in *International Conference on Machine Learning*. PMLR, 2021, pp. 12 868–12 877.

[15] Z. He, W. Wang, J. Dong, and T. Tan, "Transferable sparse adversarial attack," in *Proceedings of the IEEE/CVF Conference on Computer Vision and Pattern Recognition*, 2022, pp. 14 963–14 972.

[16] Y. Dong, H. Su, B. Wu, Z. Li, W. Liu, T. Zhang, and J. Zhu, "Efficient decision-based black-box adversarial attacks on face recognition," in *Proceedings of the IEEE/CVF Conference on Computer Vision and Pattern Recognition*, 2019, pp. 7714–7722.

[17] X. Wei, Y. Guo, and J. Yu, "Adversarial sticker: A stealthy attack method in the physical world," *IEEE Transactions on Pattern Analysis and Machine Intelligence*, vol. 45, no. 3, pp. 2711–2725, 2022.

[18] X. Wei, Y. Guo, J. Yu, and B. Zhang, "Simultaneously optimizing perturbations and positions for black-box adversarial patch attacks," *IEEE Transactions on Pattern Analysis and Machine Intelligence*, 2022.

[19] I. Evtimov, K. Eykholt, E. Fernandes, T. Kohno, B. Li, A. Prakash, A. Rahmati, and D. Song, "Robust physical-world attacks on machine learning models," *Learning*, 2017.

[20] A. Zolfi, M. Kravchik, Y. Elovici, and A. Shabtai, "The translucent patch: A physical and universal attack on object detectors," in *Proceedings of the IEEE/CVF Conference on Computer Vision and Pattern Recognition*, 2021, pp. 15 232–15 241.

[21] Z. Hu, S. Huang, X. Zhu, F. Sun, B. Zhang, and X. Hu, "Adversarial texture for fooling person detectors in the physical world," in *Proceedings of the IEEE/CVF Conference on Computer Vision and Pattern Recognition*, 2022, pp. 13 307–13 316.

[22] S. Komkov and A. Petiushko, "Advhat: Real-world adversarial attack on arcface face id system," in *2020 25th International Conference on Pattern Recognition (ICPR)*. IEEE, 2021, pp. 819–826.

[23] Y.-C.-T. Hu, B.-H. Kung, D. S. Tan, J.-C. Chen, K.-L. Hua, and W.-H. Cheng, "Naturalistic physical adversarial patch for object detectors," in *Proceedings of the IEEE/CVF International Conference on Computer Vision*, 2021, pp. 7848–7857.

[24] Y. Zhang, Y. Zhang, J. Qi, K. Bin, H. Wen, X. Tong, and P. Zhong, "Adversarial patch attack on multi-scale object detection for uav remote sensing images," *Remote Sensing*, vol. 14, no. 21, p. 5298, 2022.

[25] J. Lian, S. Mei, S. Zhang, and M. Ma, "Benchmarking adversarial patch against aerial detection," *IEEE Transactions on Geoscience and Remote Sensing*, vol. 60, pp. 1–16, 2022.

[26] A. M. M. S. T. Vladu, "Towards deep learning models resistant to adversarial attacks," *Statistics*, 2017.

[27] N. Carlini and D. Wagner, "Towards evaluating the robustness of neural networks," in *2017 IEEE Symposium on Security and Privacy (SP)*. IEEE, 2017, pp. 39–57.

[28] C. Luo, Q. Lin, W. Xie, B. Wu, J. Xie, and L. Shen, "Frequency-driven imperceptible adversarial attack on semantic similarity," in *Proceedings of the IEEE/CVF Conference on Computer Vision and Pattern Recognition*, 2022, pp. 15 315–15 324.

[29] Y. F. Fu, S. Wu, Y. Lin *et al.*, "Patch-fool: Are vision transformers always robust against adversarial perturbations?" *ICLR 2022*, 2021.

[30] X. Li and S. Ji, "Generative dynamic patch attack," *British Machine Vision Conference (BMVC)*, 2021.

[31] J.-C. Burnel, K. Fatras, R. Flamary, and N. Courty, "Generating natural adversarial remote sensing images," *IEEE Transactions on Geoscience and Remote Sensing*, vol. 60, pp. 1–14, 2021.

[32] M. Arjovsky, S. Chintala, and L. Bottou, "Wasserstein generative adversarial networks," in *International Conference on Machine Learning*. PMLR, 2017, pp. 214–223.

[33] Y. Yuan, X. Chen, and J. Wang, "Object-contextual representations for semantic segmentation," in *European Conference on Computer Vision*. Springer, 2020, pp. 173–190.

[34] Z. Shao, K. Yang, and W. Zhou, "Performance evaluation of single-label and multi-label remote sensing image retrieval using a dense labeling dataset," *Remote Sensing*, vol. 10, no. 6, p. 964, 2018.

[35] G. Hinton, O. Vinyals, and J. Dean, "Distilling the knowledge in a neural network," *Computer Science*, vol. 14, no. 7, pp. 38–39, 2015.

[36] Z. Zhao, Z. Liu, and M. Larson, "On success and simplicity: A second look at transferable targeted attacks," *Advances in Neural Information Processing Systems*, vol. 34, pp. 6115–6128, 2021.

[37] L. I. Rudin, S. Osher, and E. Fatemi, "Nonlinear total variation based noise removal algorithms," *Physica D: nonlinear phenomena*, vol. 60, no. 1-4, pp. 259–268, 1992.

[38] Z. Zhao, Z. Liu, and M. Larson, "Towards large yet imperceptible adversarial image perturbations with perceptual color distance," in *Proceedings of the IEEE/CVF Conference on Computer Vision and Pattern Recognition*, 2020, pp. 1039–1048.

[39] G.-S. Xia, J. Hu, F. Hu, B. Shi, X. Bai, Y. Zhong, L. Zhang, and X. Lu, "AID: A benchmark data set for performance evaluation of aerial scene classification," *IEEE Transactions on Geoscience and Remote Sensing*, vol. 55, no. 7, pp. 3965–3981, 2017.

[40] G. Cheng, J. Han, and X. Lu, "Remote sensing image scene classification: Benchmark and state of the art," *Proceedings of the IEEE*, vol. 105, no. 10, pp. 1865–1883, 2017.

[41] K. He, X. Zhang, S. Ren, and J. Sun, "Deep residual learning for image recognition," in *Proceedings of the IEEE Conference on Computer Vision and Pattern Recognition*, 2016, pp. 770–778.

[42] G. Huang, Z. Liu, L. Van Der Maaten, and K. Q. Weinberger, "Densely connected convolutional networks," in *Proceedings of the IEEE Conference on Computer Vision and Pattern Recognition*, 2017, pp. 4700–4708.

[43] R. Zhang, P. Isola, A. A. Efros, E. Shechtman, and O. Wang, "The unreasonable effectiveness of deep features as a perceptual metric," in *Proceedings of the IEEE conference on computer vision and pattern recognition*, 2018, pp. 586–595.

[44] D. Kingma and J. Ba, "Adam: A method for stochastic optimization," *Computer Science*, 2014.

[45] Z. Wang, J.-J. Huang, T. Liu, Z. Chen, W. Zhao, X. Liu, Y. Pan, and L. Liu, "Multi-patch adversarial attack for remote sensing image classification," in *Proceedings of The 7th APWeb-WAIM International Joint Conference on Web and Big Data*, 2023.

[46] R. R. Selvaraju, M. Cogswell, A. Das, R. Vedantam, D. Parikh, and D. Batra, "Grad-CAM: Visual explanations from deep networks via gradient-based localization," in *Proceedings of the IEEE International Conference on Computer Vision*, 2017, pp. 618–626.

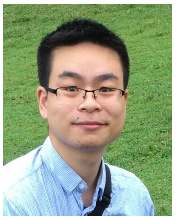

Jun-Jie Huang (Member, IEEE) received the B.Eng. (Hons.) degree with First Class Honours in Electronic Engineering and the M.Phil. degree in Electronic and Information Engineering from The Hong Kong Polytechnic University, Hong Kong, China, in 2013 and 2015, respectively, and the Ph.D. degree from Imperial College London (ICL), London, U.K., in 2019. He is an Associate Professor with College of Computer Science and Technology, National University of Defence Technology (NUDT), Changsha, China. During 2019 - 2021, he was a Postdoc with Communications and Signal Processing (CSP) Group, Electrical and Electronic Engineering Department, ICL, London, U.K. His research interests include the areas of model-based deep learning, computer vision, and signal processing.

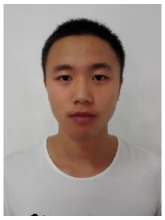

Ziyue Wang received the Bachelor's degree and the Master's degree from National University of Defense Technology (NUDT) in 2017 and 2023, respectively. His research interests include adversarial attack and remote sensing image.

Tianrui Liu received her Ph.D. degree in 2019 from Imperial College London (ICL), U.K.. She is currently an Associate Professor with the College of Computer Science and Technology, National University of Defense Technology (NUDT), China. Before that, she was a Research Associate in the BioMedIA Group of ICL. Her research interests include computer vision, machine learning and medical image/video analysis.

Wenhan Luo is an Associate Professor in the the Hong Kong University of Science and Technology. Prior to that, he worked as an Associate Professor at Sun Yat-sen University, a research scientist for Tencent and Amazon. He has published over 70 papers in top conferences and leading journals, including ICML, CVPR, ICCV, ECCV, ACL, AAAI, ICLR, TPAMI, IJCV, TIP, etc. He also has been reviewer, senior PC member and Guest Editor for several prestigious journals and conferences. His research interests include several topics in computer vision and machine learning, such as image/video synthesis, and image/video quality restoration. He received the Ph.D. degree from Imperial College London, UK, 2016, M.E. degree from Institute of Automation, Chinese Academy of Sciences, China, 2012 and B.E. degree from Huazhong University of Science and Technology, China, 2009.

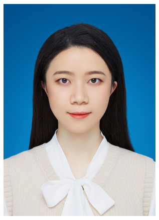

Zihan Chen received the Bachelor's degree from Lanzhou University in 2021, and the Master's degree from National University of Defense Technology (NUDT), in 2023. She is currently pursuing the Ph.D. degree with NUDT. Her research interests include computer vision and information hiding.

Wentao Zhao received the Ph.D. degree from the National University of Defense Technology (NUDT), in 2009. He is now a professor with the National University of Defense Technology. His research interests include network performance optimization, information processing and machine learning. Since 2011, he has been serving as a member of Council Committee of Postgraduate Entrance Examination of Computer Science and Technology, NUDT. He has edited one book entitled "Database Principle and Technology" and several technical papers such as Communications of the CCF, AAAI, IJCAI, FAW, etc.

Meng Wang (Fellow, IEEE) received the B.E. and Ph.D. degrees in the special class for the gifted young from the Department of Electronic Engineering and Information Science, University of Science and Technology of China, Hefei, China, in 2003 and 2008, respectively. He is currently a Professor with the Hefei University of Technology, China. He has authored over 200 book chapters, journals, and conference papers in his research areas. His current research interests include multimedia content analysis, computer vision, and pattern recognition. He was a recipient of the ACM SIGMM Rising Star Award 2014. He is an Associate Editor of the IEEE Transactions on Knowledge and Data Engineering, the IEEE Transactions on Circuits and Systems for Video Technology, and the IEEE Transactions on Neural Networks and Learning Systems.